Journal of Applied Physics

Investigation of electronic structure and optical properties of thallium lead halides: First principle calculations

Cite as: J. Appl. Phys. **124**, 093102 (2018); https://doi.org/10.1063/1.5045171
Submitted: 18 June 2018 . Accepted: 20 August 2018 . Published Online: 05 September 2018

Asad Mahmood, Gansehng Shi, Jing Sun, and Jianjun Liu

JOURNAL OF APPLIED PHYSICS **124**, 093102 (2018)

Investigation of electronic structure and optical properties of thallium lead halides: First principle calculations

Asad Mahmood,[a] Gansehng Shi, Jing Sun,[b] and Jianjun Liu
The State Key Lab of High Performance Ceramics and Superfine Microstructure, Shanghai Institute of Ceramics, University of Chinese Academy of Sciences, 1295 Dingxi Road, Shanghai 200050, People's Republic of China

(Received 18 June 2018; accepted 20 August 2018; published online 5 September 2018)

Using first principle calculations, we comprehend the electronic structure and optical constant of thallium lead halides TI_3PbX_5 (X = Cl, Br, I), which are viewed as potential materials for mid-infrared and near-infrared applications. The generalized gradient approximation function given by Perdew-Burke-Ernzerhof is used for geometry optimization and properties calculations. The calculated Mulliken charges are more positive for Pb than TI in the TI_3PbCl_5 system demonstrating a high electronic density contribution from the Pb-Cl bonds in contrast to the TI-Cl bonds. Similarly, the TI_3PbCl_5 configuration displays the smallest enthalpy value suggesting a more stable structure among different TI_3PbX_5 species studied in this work. The band gap value for TI_3PbCl_5 has been calculated as 3.52 eV, which decreases to 3.14 eV and 2.64 eV for the TI_3PbBr_5 and TI_3PbI_5, respectively. Additionally, the TI_3PbI_5 exhibits a high magnitude of real component of static dielectric function $\varepsilon_1(k)$ in contrast to TI_3PbBr_5 and TI_3PbCl_5. The optical absorption results display a redshift when TI_3PbCl_5 is doped with Br and I sequentially. These outcomes suggest that the concentration of halide elements can be adjusted to enhance the optical properties of TI_3PbX_5 for optoelectronic device applications. *Published by AIP Publishing.*
https://doi.org/10.1063/1.5045171

I. INTRODUCTION

The progress in non-linear optical crystals for mid-infrared (MIR = 3–12 μm) laser sources provides widespread opportunities for applications in cutting edge technologies, such as space based communication systems, medical diagnostics, and remote sensing.[1] The challenge with such materials is the scaling down of particle size so that it can be compacted in small volumes while considering characteristics such as hygroscopicity, stability, and energy/power output. Previously, rare-earth chlorides (i.e., Pr^{3+}: $LaCl_3$) lasing at 2.34 and 4.31 μm (Ref. 2) and chalcogenides (i.e., Dy^{3+}: $CaGa_2S_4$) lasing at 3.2 and 7.2 μm (Ref. 3) have been considered as potential materials for MIR applications; however, these materials are exceedingly hygroscopic, which impede their usefulness in the development of laser sources.[2] Therefore, an increasing attention has been given to synthesize new non-hygroscopic counterparts for MIR laser applications. Along these lines, thallium lead halides have shown remarkable potential for next generation optical and electrical applications. Thallium lead halide species with a stoichiometric formula of A_3BX_5 (A = TI; B = Pb; and X = Br, I, Cl) have emerged as new technological materials.[4] These materials exhibit a perovskite (ABO_3) crystal structure, which provide prospects to control their crystal morphology through processing and doping to achieve superior optical and electrical properties. In this manner, TI_3PbBr_5 and TI_3PbCl_5 have been studied for applications such as MIR and near-IR nonlinear optical effects.[5,6] Likewise, rare-earth elements doped TI_3PbBr_5 has demonstrated an outstanding potency for MIR solid-state lasers.[6] The presence of heavy lead ion in the crystal lattice structure of these materials is accounted for rendering hyper polarizability values.[7] Additionally, it is predicted that the quantum dots of A_3BX_5 based materials will demonstrate superior properties for photonic applications.[8] Despite the fact that these materials could prove as potential candidates in device performance of various optical and electrical applications, A_3BX_5 based perovskite structures have been rarely studied. Initially, Keller[9] studied the crystalline structure of TI_3PbCl_5 single crystal and calculated the cell parameters; however, the assigned space group ($P4_1$) was not confirmed by the latter's work. Skarstad *et al.*[10] synthesized single crystals of TI_3PbCl_5 using the Bridgman method and reported a non-centrosymmetric space group $P4_12_12$ (No. 92), exhibiting a tetragonal symmetry containing four formula units per unit cell. This study has been further confirmed by X-ray single crystal diffraction measurements.[11] Additionally, the first order phase transition of TI_3PbCl_5 has been reported as 155 °C (Ref. 12) corresponding to the ordering of TI^+ and Pb^{2+} cations leaving an unaffected position of Cl^- anions. Another attempt was reported by Ferrier *et al.*[11] who determined the phase transition temperature as 171 °C for Ti_3PbCl_5; however, they could not determine the exact phase transition temperature. Similarly, Khyzhun *et al.*[13] studied the electronic structure and chemical stability of TI_3PbBr_5 single crystals grown by using the Bridgman-Stockalgar method. An X-ray photoelectron core-level and valence band (VB) spectrum were generated for the pristine and Ar^+-ions irradiated surfaces. Moreover, the total and partial density of

[a]E-mail: amkhan036@yahoo.com
[b]E-mail: jingsun@mail.sic.ac.cn

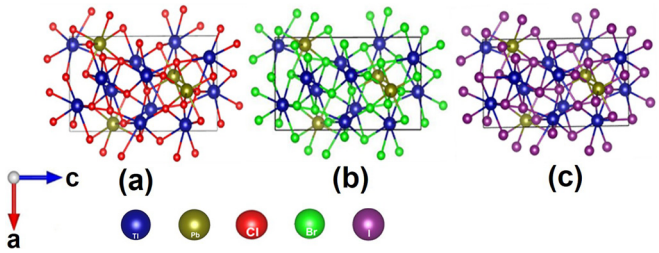

FIG. 1. Schematic of geometrically optimized structures of TI_3PbX_5 (X = Cl, Br, I) using GGA and PBE method.

states (PDOS) of the product materials were calculated using the full potential linearized augmented plane wave (FP_LAPW) based method. The low temperature (LT) TI_3PbBr_5 data suggested that Br 4p-like states dominated the VB contributing mainly to the top and central region of the VB. The TI 6s-and TI 6p-like states were observed to contribute in the bottom of the conduction band (CB).

Despite various studies directed on thallium lead halides, no study reports a detailed first principal investigation of the electronic microstructure and optical properties of A_3BX_5 analogs. In this paper, we have implemented first principle calculations to contemplate the electronic structure and optical properties of thallium lead halide species containing Cl, Br, and I. The geometric structures, formation energies, absorption properties, dielectric functions, and total and partial density of stets have been analyzed to study the effect of varying the halide group in the host crystal structure of thallium lead halide.

II. COMPUTATIONAL DETAILS

The modeled structures of TI_3PbX_5 (X = Cl, Br, I) were optimized using first principal calculations. The generalized gradient approximation (GGA) function given by Perdew-Burke-Ernzerhof (PBE) was used to treat all electronic energy of exchange correlation for geometry optimization and properties calculations.[14] Additionally, an ultrasoft pseudopotential and Broyden–Fletcher–Goldfarb–Shanno (BFGS) algorithm was utilized in all calculations.[15,16] At first, the lattice parameters a = 8.716 Å, b = 9.241 Å, and c = 15.687 Å and $\alpha = \beta = \gamma = 90.000°$ were used to build the TI_3PbCl_5 primitive cell using an orthorhombic crystal system exhibiting a space group of $P2_12_12_1$ (point group = 222). After geometry optimization, Cl was replaced with Br and I atoms sequentially to construct the TI_3PbBr_5 and TI_3PbI_5, respectively. A periodically repeated super cell $2 \times 2 \times 2$ large enough to approximate the physical properties was used for geometry optimization and properties calculations. The following convergence parameters were used to relax the structures and optical constant calculations including: (a) maximum force = 0.03 eV/atom, (b) energy tolerance factor = 1.0×10^{-5} eV/atom, (c) maximum stress = 0.05 GPa, and (d) maximum displacement = 0.001 Å. We used an energy cut-off (340.0 eV) high enough to fully converge the properties and self-consistent function (SCF) 1.0×10^{-6} eV/atom as the electron parameters. A $1 \times 1 \times 1$ k point sample set was used for geometry optimization and calculations of density of states. The electronic configurations used for the elements were TI: $[Xe]\ 6s^2\ 4f^{14}\ 5d^{10}\ 6p^1$, Pb: $[Xe]\ 4f^{14}\ 5d^{10}\ 6s^2\ 6p^2$, Cl: $[Ne]\ 3s^2\ 3p^6$, Br: $[Ar]\ 4s^2\ 3d^{10}\ 4p^5$, and I: $[Kr]\ 4d^{10}\ 5s^2\ 5p^5$.

III. RESULTS AND DISCUSSION

A. Geometric structure

The geometrically optimized TI_3PbX_5 (X = Cl, Br, I) structure configurations are given in Figs. 1(a)–1(c). The corresponding lattice parameters, enthalpy, and Mullikan charges are given in Table I. A significant increment in the lattice parameters can be observed when the Cl is replaced by Br and I, which is related to the ionic radii of Br and I. The ionic radii of Br (1.96 Å) and I (2.2 Å) are larger in contrast to the ionic radius of Cl (1.81 Å). Subsequently, the substitution of Br and I successively expands the crystal lattice and hence increases the lattice parameters. The average Pb-halide bond length of 2.8933 Å has been calculated in the TI_3PbCl_5 crystal system. The corresponding average Pb-halide bond length for TI_3PbBr_5 and TI_3PbI_5 configurations increases to 2.9550 Å and 3.1606 Å, respectively, causing the cell to swell. In addition, we calculated the Mulliken charges to understand the electron density sheared by an atom in the TI_3PbX_5 crystal system. The more positive the Mulliken charge value is for an atom, the higher its electron density contribution is in the crystal system. The calculated Mulliken charge value for Pb is more positive compared to TI in the TI_3PbCl_5 crystal system suggesting more charge density contribution by Pb to form Pb-Cl bonds in contrast to TI-Cl bonds. Furthermore, no significant charge variation is observed for the Cl atoms in contrast to TI. Pb atoms lacking charge variation suggest that TI has a greater influence on altering the charge. A similar behavior is observed in the TI_3PbBr_5 and TI_3PbI_5 configurations. To compare the structure stability, we calculated enthalpy. The corresponding enthalpy values indicate that the geometric configuration of TI_3PbCl_5 is the most stable structure in all of the three TI_3PbX_5 species studied in this work.

TABLE I. Calculated cell parameters, enthalpy, and average Mullikan charges for TI_3PbX_5 (X = Cl, Br, I) configurations.

	Cell parameters				Mullikan charges (Avg.)				
Configuration	A	b	C	Enthalpy (eV)	TI	Pb	Cl	Br	I
TI_3PbCl_5	8.4205	8.8401	15.1377	−87954.8	0.53	0.90	−0.49	…	…
TI_3PbBr_5	8.7161	9.2413	15.6868	−88768.7	0.28	0.52	…	−0.27	…
TI_3PbI_5	9.1279	9.8622	16.6170	−95412.4	0.28	0.42	…	…	−27

B. Electronic properties

Figure 2 shows the calculated band structures and PDOS ranging from −5 to 5 eV for the TI_3PbX_5 (X = Cl, Br, I) species with the Fermi level (E_F) set to 0. The results suggest significant variations in the band gap values corresponding to different halide elements in the structural models studied. The band gap value for TI_3PbCl_5 is 3.52 eV, which decreases to 3.14 eV and 2.64 eV for TI_3PbBr_5 and TI_3PbI_5 configurations, respectively. The calculated band gap values are in good agreement with the experimental results.[17] Generally, the density functional theory (DFT) calculations undermine the band gap values due to termination of the DFT in GGA.[18] However, such discrepancies can be corrected by using the Hubbard-like term (U) utilizing DFT + U in order to treat the strong on-site Coulomb interaction of electrons that are underestimated by the local-density approximation (LDA) and GGA.[19,20] The application of U in DFT requires an expensive calculation time, which was unfortunately not available on our premises. Despite this drawback, the results can still be understood and the optical properties can be compared efficiently. A closer observation of the calculated band dispersion in TI_3PbCl_5 for several symmetry directions suggests that the VB maxima (VBM) and CB minima (CBM) are not located at the same point which is characteristic of indirect band gap semiconductor materials. The TI_3PbBr_5 and TI_3PbI_5 configurations demonstrate a similar behavior. These results correlate with previously published works[1] and references therein. It can be seen that the corresponding band structure is very dense with respect to energy, containing many electron states. A close observation of the VB suggests a weak band dispersion, which results in somewhat flat electronic bands. This behavior causes low mobility of holes. Moreover, the CB also demonstrates a narrow band distribution; however, it is more pronounced in comparison to the VB, indicating more electron mobility in the CB. Based on this, it can be inferred that the electron mobility in the CB is higher than the holes in the VB. This characteristic of materials is important for applications including light emitting diodes and solar cells.

The PDOS for various elements are given in Fig. 3 ranging from −20 to 20 eV. The VB ranging from −10 to 0.3 eV for TI_3PbCl_5 can be divided into the upper VB (−3.01 to 0 eV) and lower VB (−3.01 to −10 eV). The upper core TI-6p generates somewhat broader bands extending from 3.2 to 7.5 eV in the CB; however, the TI-6s demonstrates a narrow band in the VB and comparatively a broader band in the CB in the range of 8.2 to 18.7 eV. Similarly, Pb-6p (3.1 to 7.3 eV) and 6s (8.3 to 18.4 eV) like states generate broader bands in the CB and somewhat narrow bands in the VB. The TI-5d and Pb-5d like states develop sharp narrow bands in the lower VB region, while no significant contribution can be seen in the upper VB and CB. It can be noted that the Cl-3p states, Pb-6s states, and TI-6s states mainly contribute to the upper VB, while a small contribution can be traced from the TI-6s and Pb-6s like states in this region. However, no contribution is detected from the Cl-3s states. The TI-5d states contribute only in the lower VB at around −10 eV. Similarly, the TI-6p and Pb-5p like states mainly contribute to the CB, which extends in this region (3.25 to 18.266 eV). Furthermore, the CB can be divided into lower CB (3.25 to 7.41 eV) and higher CB (8.33 to 17.87 eV). A small contribution from TI-6s and Pb-6s like states can also be traced in this region. Similar results were observed for Br and I containing configurations; however, Br-4s and I-5s demonstrate a significant contribution in the conduction band in contrast to TI_3PbCl_5.

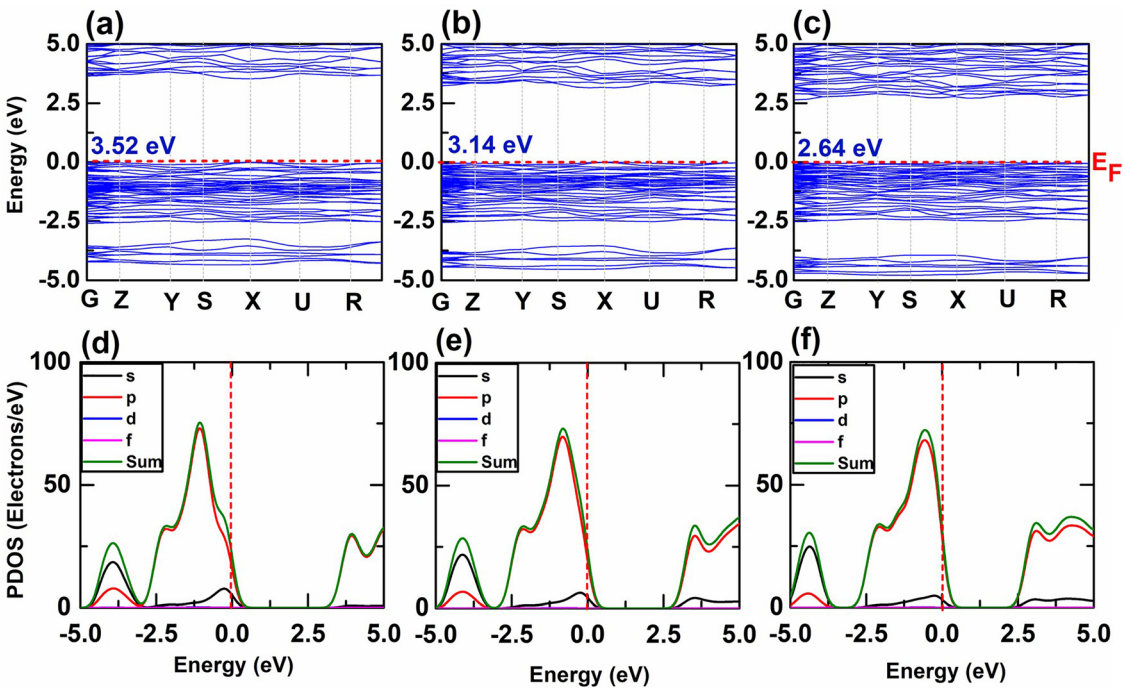

FIG. 2. Calculated band structure, band gap energies, and total and partial densities of states for TI_3PbX_5 (X = Cl, Br, I) using GGA and PBE method. The Fermi level is set to 0 eV on the energy axis as denoted by dotted red line.

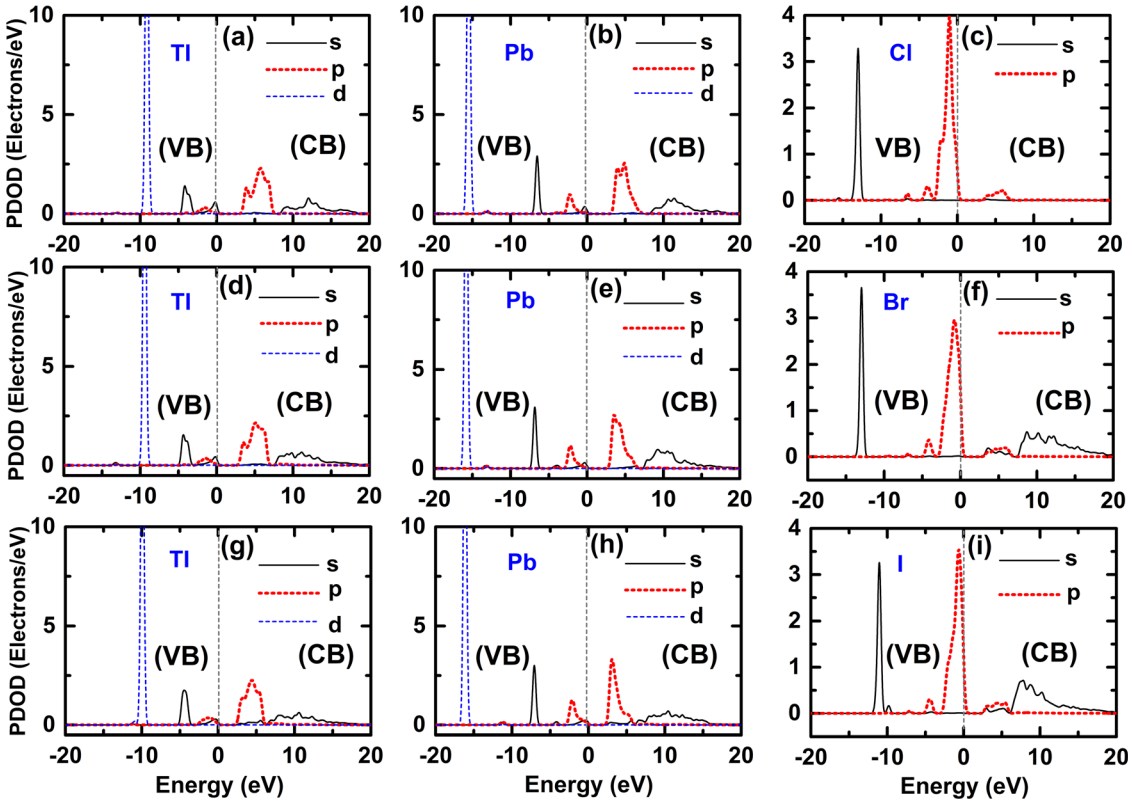

FIG. 3. The partial density of states for TI_3PbX_5 (X = Cl, Br, I) using GGA and PBE method demonstrating individual elements contributions in the valance and conduction band.

C. Optical properties

The optical constants are of high significance to outline materials showing superior optoelectrical properties for different applications including transparent conductive layers (TOCs),[21,22] mid and near infra-red lasers,[23] metal-semiconductor-insulator diodes,[24] thin film transistors,[25] and ultraviolet detectors.[26] The interaction of photon with an electron in the ground state is depicted as the time dependent perturbation of the ground electronic state. The corresponding absorption or emission of photon causes the electronic transition between the occupied and vacant states. This excitation phenomenon produces a spectrum, which is considered as the joint density of states between the VB and CB.[27] The complex dielectric function given in the following equation can be used to study the optical properties of materials:

$$\varepsilon(\omega) = \varepsilon_1 + i\varepsilon_2, \tag{1}$$

where ε_1 and ε_2 are the real and imaginary components of dielectric functions, respectively, while ω represents the photon frequency. The joint DOS and the momentum matrix function can be used to calculate the magnitude of $\varepsilon_2(\omega)$ from the electronic structure using the following equation:[28]

$$\varepsilon_2(q \to O_{\hat{u},\hbar\omega}) = \frac{2\pi e^2}{\Omega\varepsilon_0} \sum\nolimits_{k,v,c} I\langle\psi_k^c|u.r|\psi_k^v\rangle|^2 \delta\left(E_k^c - E_k^v - E\right), \tag{2}$$

where k is reciprocal lattice, u is incident electric field polarization, and v and c are valance and conduction bands, respectively. Along these lines, the Kramer-Kroning relation can be used to calculate the real part of dielectric function $(\varepsilon_1(\omega))$

$$\varepsilon_1 = 1 + \frac{2}{\pi} M \int_0^{\alpha} \frac{\varepsilon_{2(\acute{\omega})\acute{\omega}}}{\acute{\omega}^2 - \omega^2} d\omega. \tag{3}$$

Moreover, the other optical parameters including reflectivity $R(\omega)$, refractive index $n(\omega)$, dielectric loss function $L(\omega)$, and absorption $\propto(\omega)$ properties are calculated using $\varepsilon_1(\omega)$ and $\varepsilon_2(\omega)$ values.[29] The following equations are used to calculate the above-mentioned properties:

$$\propto(\omega) = \sqrt{2}\omega\left[\sqrt{\varepsilon_1^2(\omega) + \varepsilon_1^2(\omega)} - \varepsilon_1(\omega)\right]^{\frac{1}{2}}, \tag{4}$$

$$R(\omega) = \frac{(n-1)^2 + k^2}{(n+1)^2 + k^2,} \tag{5}$$

$$n(\omega) = \left[\sqrt{\varepsilon_1^2(\omega) + \varepsilon_1^2(\omega)} + \varepsilon_1(\omega)\right]^{\frac{1}{2}} \Big/ \sqrt{2}, \tag{6}$$

$$L(\omega) = \frac{\varepsilon_2(\omega)}{\left[\varepsilon_1^2(\omega) + \varepsilon_2^2(\omega)\right]}. \tag{7}$$

The calculated optical constants are given in Table II. The real and imaginary parts of the dielectric function are given in Fig. 4. The TI_3PbI_5 configuration demonstrates a high magnitude for $\varepsilon_1(\omega)$ at zero frequency in contrast to TI_3PbBr_5 and TI_3PbCl_5 configurations. These results agree with the model proposed by Penn,[17] suggesting an inverse

TABLE II. Calculated values of static refractive index, real component of dielectric function, reflectivity, and loss function at bulk plasma frequency for TI_3PbX_5 (X = Cl, Br, I) configurations.

	Optical functions			
Configuration	n (0)	ε_1 (k)	L $(\omega)_{Wp}$	R (0)
TI_3PbCl_5	2.22	4.91	2.29	0.143
TI_3PbBr_5	2.44	5.78	1.86	0.170
TI_3PbI_5	5.66	31.43	2.58	0.496

relationship between the energy band gap and static dielectric constant ε_1(k). This relationship is supported by the energy band gap results for TI_3PbX_5, where the band gap values decrease in the order $TI_3PbCl_5 > TI_3PbBr_5 > TI_3PbI_5$. The magnitude of $\varepsilon_1(\omega)$ is observed to increase, reaching a maximum value such as 12.097 at 2.80 eV for TI_3PbI_5. A similar trend is detected for TI_3PbBr_5 and TI_3PbCl_5 as 10.25 at 3.33 eV and 8.64 at 3.33 eV, respectively. The $\varepsilon_2(\omega)$ values, related to the optical absorption of materials, increase rapidly from the band gap values of 3.52, 3.14, and 2.64 eV for TI_3PbX_5 species doped with Cl, Br, and I, reaching a maximum at 5.17, 4.39, and 3.8 eV for Cl, Br, and I doped configurations, respectively. Additionally, the spectrum can be divided into three distinct peaks for all the structural models. The lowest energy peaks (5.11, 4.39, and 3.77 eV for Cl, Br, and I, respectively) are related to the electronic transition from the upper VB to the lower CB. The second energy peaks at around 10.39, 9.42, and 7.92 eV (Cl, Br, and I, respectively) are consistent with the electronic transitions between the 3d- and 2p-states in the VB. The corresponding peaks significantly shifted to the low energy region for I. These results suggest that variation in the halide group of TI_3PbX_5 strongly influences their optical properties; hence, they can be used to manipulate these properties.

The energy loss function is given in Fig. 5, which demonstrates the energy lost by an electron accelerating through a material. Generally, the energy loss in the region to 50 eV is associated with plasmons while the energy loss beyond 50 eV is caused by excitations in the inner shell. The predominant peaks for Cl doped configuration appear at 8.45, 12.48, 18.58, 20.93, and 26.75 suggesting high energy plasmons in the perovskites. The peaks shift to low energy regions for Br and I doped configurations suggesting an increasing number of plasmons with the replacement of Cl. The main peak in the plot regarded as the bulk plasma peak, Wp, results when $\varepsilon_2(\omega) < 1$ and $\varepsilon_1(\omega)$ approaches 0. The

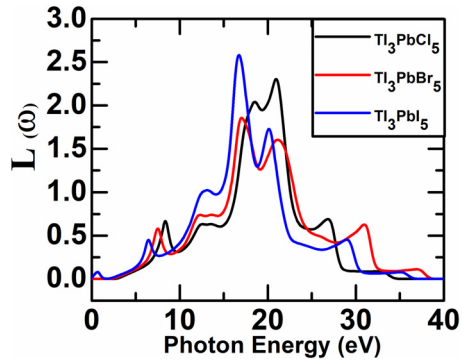

FIG. 5. Calculated loss-energy function for TI_3PbX_5 (X = Cl, Br, I) configurations.

peak intensity generally corresponds to the order-disorder behavior of a crystal. In the current study, a high peak intensity is seen for TI_3PbI_5, which shows that iodine doping results in comparatively more disorder than Cl or Br doping. These results suggest that the degree of order in pure Br doped configuration is the highest.

Figures 6(a) and 6(b) show the reflectivity and refractive index function of energy. The percentage of reflectivity for the I-doped configuration is high compared to Br and Cl doped configurations, which decrease significantly. The corresponding static reflectivity values are recorded as 0.143, 0.170, and 0.496 for Cl, Br, and I based models. The maximum reflectivity peaks at non-zero frequency are observed to be 4.99, 5.84, and 6.58 eV for I, Br, and Cl based configurations. Additionally, the reflectivity peaks are shifted to low photon energy for the I-doped model. The curve behavior for the n(ω) significantly varied for all of the TI_3PbX_5 species. It is clear from Fig. 6(b) that the n(ω) curves shift to low energy regions for Br and I doped configurations. Similarly, an increase in the n(ω) is observed below the energy band gap values to a maximum value of 3.02, 3.28, and 3 at 4.11, 3.36, and 3.00 eV for Cl, Br, and I doped models. The corresponding static n(ω) and static ε_1(k) values are related by equation: $n(0) = \sqrt{\varepsilon 1(0)}$, which are satisfied in our calculations for the TI_3PbX_5 models. The significant variation observed in n(ω) values by replacing halide groups provides an opportunity to manipulate the optical properties by doping different concentrations of thallium lead halides. Additionally, the variation is more pronounced in the low energy region in contrast to the high energy region. Therefore, it can be inferred that as the external pressure and phase transition is more pronounced in the low energy region.

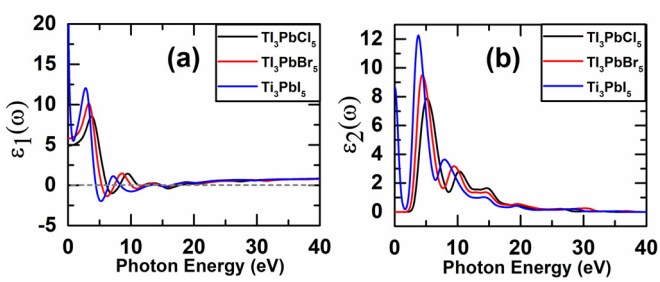

FIG. 4. Calculated dielectric functions containing the real (a) and imaginary (b) components for TI_3PbX_5 (X = Cl, Br, I) configurations.

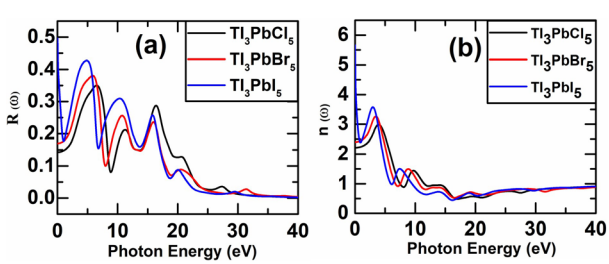

FIG. 6. Calculated reflectivity (a) and refractive index (b) for TI_3PbX_5 (X = Cl, Br, I) configurations.

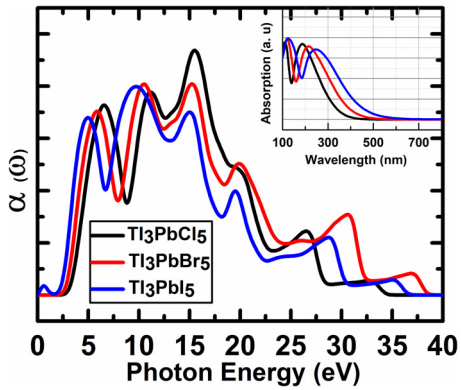

FIG. 7. Calculated absorption functions for TI_3PbX_5 (X = Cl, Br, I) configurations.

The absorption coefficient spectra (Fig. 7) for TI_3PbX_5 show a wide absorption band starting at around the computed band gap values and increasing up to 34.6, 36.6, and 38.65 eV for Cl, I, and Br, respectively. The TI_3PbCl_5 shows three distinct peaks around 6.48, 11.10, and 15.14, at 19.93, 26.52, and 33.04 eV, respectively. The peaks around 10 eV are called the vacuum ultraviolet region. It is clear that the replacement of Cl by Br and I significantly shifts the peaks to low energy. The results suggest a red shift, which is evident in the absorption versus frequency graph (inset figure of Fig. 7).

IV. CONCLUSIONS

In summary, we have applied the density functional theory to comprehend the electronic structure and optical properties of thallium lead halides in detail. The variation in halide elements from Cl to Br and I significantly affected the electronic band gap and optical properties of thallium lead halide crystal systems. The band gap was observed to decrease from 3.52 eV (Cl) to 3.14 eV (Br) and 2.64 eV (I). The calculated enthalpy values suggest that the Cl doped configuration is the most stable structure in contrast to Br and I doped configurations. The lattice parameters also demonstrate a significant increase by the addition of Br and I. The optical constant study suggests a variation in the low energy region. Based on this evidence, it can be inferred that by adjusting proper stoichiometric concentrations of the halide group elements (Cl, Br, and I), these elements can be used to manipulate the structure and therefore, the optical and electrical properties of these materials for practical device applications.

ACKNOWLEDGMENTS

There are no conflicts to declare.

[1]V. L. Bekenev, O. Y. Khyzhun, A. K. Sinelnichenko, V. V. Atuchin, O. V. Parasyuk, O. M. Yurchenko, Y. Bezsmolnyy, A. V. Kityk, J. Szkutnik, and S. CaŁus, J. Phys. Chem. Solids **72**, 705 (2011).
[2]S. R. Bowman, L. B. Shaw, B. J. Feldman, and J. Ganem, IEEE J. Quantum Electron. **32**, 646 (1996).
[3]L. Isaenko, A. Yelisseyev, A. Tkachuk, S. Ivanova, S. Vatnik, A. Merkulov, S. Payne, R. Page, and M. Nostrand, Mater. Sci. Eng. B **81**, 188 (2001).
[4]P. Vashishtha, D. Z. Metin, M. E. Cryer, K. Chen, J. M. Hodgkiss, N. Gaston, and J. E. Halpert, Chem. Mater. **30**, 2973 (2018).
[5]A. Ferrier, M. Velázquez, X. Portier, J.-L. Doualan, and R. Moncorgé, J. Cryst. Growth **289**, 357 (2006).
[6]A. Ferrier, M. Velázquez, J. L. Doualan, and R. Moncorgé, Appl. Phys. B **95**, 287 (2009).
[7]N. B. Singh, D. R. Suhre, K. Green, N. Fernelius, and F. K. Hopkins, Proc. SPIE **5912**, 591203 (2005).
[8]A. Ferrier, M. Velázquez, J.-L. Doualan, and R. Moncorgé, J. Lumin. **129**, 1905 (2009).
[9]V. H.-L. Keller, Z. Anorg. Allg. Chem. **432**, 141 (1977).
[10]P. M. Skarstad, C. R. Hubbard, R. S. Roth, and H. S. Parker, J. Solid State Chem. **30**, 65 (1979).
[11]A. Ferrier, M. Velázquez, O. Pérez, D. Grebille, X. Portier, and R. Moncorgé, J. Cryst. Growth **291**, 375 (2006).
[12]H.-L. Keller, J. Solid State Chem. **48**, 346 (1983).
[13]O. Y. Khyzhun, V. L. Bekenev, O. V. Parasyuk, S. P. Danylchuk, N. M. Denysyuk, A. O. Fedorchuk, N. AlZayed, and I. V. Kityk, Opt. Mater. **35**, 1081 (2013).
[14]J. P. Perdew, J. A. Chevary, S. H. Vosko, K. A. Jackson, M. R. Pederson, D. J. Singh, and C. Fiolhais, Phys. Rev. B **46**, 6671 (1992).
[15]J. D. Head and M. C. Zerner, Chem. Phys. Lett. **122**, 264 (1985).
[16]R. Fletcher, *Practical Methods of Optimization*, 2nd ed. (John Wiley & Sons, New York, 1987).
[17]D. R. Penn, Phys. Rev. **128**, 2093 (1962).
[18]S. Lany and A. Zunger, Phys. Rev. B **78**, 235104 (2008).
[19]P. Erhart, K. Albe, and A. Klein, Phys. Rev. B **73**, 205203 (2006).
[20]A. T. Raghavender, M. C. Varma, S. Deb, and N. H. Hong, AIP Conf. Proc. **1832**, 120012 (2017).
[21]K. Zilberberg, F. Gasse, R. Pagui, A. Polywka, A. Behrendt, S. Trost, R. Heiderhoff, P. Görrn, and T. Riedl, Adv. Funct. Mater. **24**, 1671 (2014).
[22]J. Halim, M. R. Lukatskaya, K. M. Cook, J. Lu, C. R. Smith, L. A. Naslund, S. J. May, L. Hultman, Y. Gogotsi, P. Eklund, and M. W. Barsoum, Chem. Mater. **26**, 2374 (2014).
[23]H. Lu, Y. Peng, H. Ye, X. Cui, J. Hu, H. Gu, A. N. Khlobystov, M. A. Green, P. J. Blower, P. B. Wyatt, W. P. Gillin, and I. Hernandez, Sci. Rep. **7**, 5066 (2017).
[24]V. Chakraborty, B. Mukhopadhyay, and P. K. Basu, Semiconductors **49**, 836 (2015).
[25]Y. Yuan, G. Giri, A. L. Ayzner, A. P. Zoombelt, S. C. Mannsfeld, J. Chen, D. Nordlund, M. F. Toney, J. Huang, and Z. Bao, Nat. Commun. **5**, 3005 (2014).
[26]Y. Wang, W. Han, B. Zhao, L. Chen, F. Teng, X. Li, C. Gao, J. Zhou, and E. Xie, Sol. Energy Mater. Sol. Cells **140**, 376 (2015).
[27]R. Schuster, C. Habenicht, M. Ahmad, M. Knupfer, and B. Büchner, Phys. Rev. B **97**, 041201(R) (2018).
[28]H. Ehrenreich and M. H. Cohen, Phys. Rev. **115**, 786 (1959).
[29]M. FOX, *Optical Properties of Solids* (Oxford University Press, New York, 2001).